Available online at www.sciencedirect.com
ScienceDirect
Journal of Solid State Chemistry 180 (2007) 2942–2949
JOURNAL OF SOLID STATE CHEMISTRY
www.elsevier.com/locate/jssc

The iron potassium diarsenate $KFeAs_2O_7$ structural, electric and magnetic behaviors

N. Ouerfelli[a], A. Guesmi[a,*], P. Molinié[b], D. Mazza[c], M.F. Zid[a], A. Driss[a]

[a]*Laboratoire de Matériaux et Cristallochimie, Faculté des Sciences, El Manar, 2092 Tunis, Tunisia*
[b]*Institut des Matériaux Jean Rouxel, UMR CNRS 6502, 2 rue de la Houssinière, BP 32229, 44322 Nantes Cedex 03, France*
[c]*Dipartimento di Scienza dei Materiali e Ingegneria Chimica, Politecnico di Torino, Corso Duca degli Abruzzi 24, 10129 Torino, Italy*

Received 3 May 2007; received in revised form 27 July 2007; accepted 10 August 2007
Available online 28 August 2007

Abstract

Crystals of a new potassium iron (III) diarsenate ($KFeAs_2O_7$) have been grown and characterized by single crystal X-ray diffraction. It crystallizes in the triclinic space group $P\bar{1}$, with $a = 7.662(1)$ Å, $b = 8.402(2)$ Å, $c = 10.100(3)$ Å, $\alpha = 90.42(3)^\circ$, $\beta = 89.74(2)^\circ$, $\gamma = 106.39(2)^\circ$, $V = 623.8(3)$ Å^3 and $Z = 4$. The final agreement factors are $R = 0.0342$, w$R = 0.0889$, $S(F^2) = 1.01$; the structural model is validated by bond valence sum (BVS) and charge distribution (CD) methods. The structure consists of corner-sharing FeO_6 octahedra and As_2O_7 diarsenate groups, the three-dimensional framework delimits tunnels running along [0 1 0] direction where the potassium ions reside. The crystal structure of the title compound is different from that of the monoclinic $KAlP_2O_7$ type but structural relationships exist between the frameworks. Impedance measurements (frequency/temperature ranges: 5–13,000 Hz/526–668 K) show $KFeAs_2O_7$ an ionic conductor being the conductivity 2.76×10^{-7} S cm^{-1} at 568 K and E_a is 0.47 eV. The BVS model suggests that the most probable potassium conduction pathway is along *b*-direction. Magnetic measurements reveal the Curie—Weiss type paramagnetic behavior over the range 30–300 K and ferromagnetic below 29.3 K.

Keywords: X-ray diffraction; Crystal structure; Charge distribution; Bond valence analysis; Ionic conductivity; Magnetic properties

1. Introduction

The metal phosphates and arsenates with general formula $A^IM^{III}X_2O_7$ (X = P, As) show a variety of crystal structure types that are controlled by the stereochemical behaviors of the A and M cations. They affect the coordination numbers, the degree of distortion of the coordination polyhedra and the conformation of the X_2O_7 groups. The crystal symmetry is then affected; it is triclinic, P-1 with two formulas per unit cell in $TlFe_{0.22}Al_{0.78}As_2O_7$ [1] and four in $AInAs_2O_7$ (A = Tl, Rb and NH_4) [2], the structure of $NaFeP_2O_7$ and isotypic compounds is monoclinic [3–7]. Some of these compounds are with high symmetry such as $NaCeP_2O_7$ [8] and KYP_2O_7 [9].

We have recently reported the synthesis and the crystal structure of $TlFe_{0.22}Al_{0.78}As_2O_7$ and we have studied the electrical properties [1]. The present paper is an extension of our work on the exploration of A–M–As–O crystallographic systems (A: monovalent, M: transition metal, mainly Fe). The electrical behavior of this material, like its ionic conductivity and magnetic susceptibility can be related to the described structural model.

2. Experimental section

Single crystals of the title compound were prepared from a mixture of KNO_3 (Fluka, 99.0%), $Fe(NO_3)_3 \cdot 9H_2O$ (Fluka, 99.0%) and H_3AsO_4 (Prolabo, 80% density 2 Mg m^{-3}), with a K:Fe:As molar ratio of 1:0.1:2. The small quantity of iron served, after many attempts, for the crystallization of single crystals with a good quality. The reagents were dissolved in an aqueous solution which has been then evaporated to dryness and the residue,

*Corresponding author. Fax: +216 71 885 008.
E-mail addresses: gabderrahmen@yahoo.fr, abderrahmen.guesmi@ipeim.rnu.tn (A. Guesmi).

0022-4596/$ - see front matter © 2007 Elsevier Inc. All rights reserved.
doi:10.1016/j.jssc.2007.08.011

placed in alumina crucible, has been slowly annealed in air to 400 °C and kept at this temperature for 24 h, in order to eliminate volatile products. In a second step, the finely ground product has been progressively heated at 700 °C for 3 h. Finally, it was cooled to 650 °C/12 h and quenched to room temperature. The obtained beige single crystals were removed from the flux matrix with boiling water. A qualitative energy dispersive spectroscopy (EDX) analysis, performed on JEOL-JSM 5400 scanning electron microscope, revealed the presence of only K, Fe, As and O elements and, within the detection limit of the instrument, verified the absence of other elements such as aluminum in the crystals.

The IR spectrum for potassium iron (III) diarsenate ($KFeAs_2O_7$) was recorded at room temperature, on a Perkin-Elmer FTIR Paragon 1000 PC spectrometer, over the range 1400–400 cm^{-1} using the KBr disk method. We have obtained the polycrystalline powder for ionic conductivity and magnetic measurements by grinding the selected single crystals after separating from the excess flux; its purity has been checked by X-ray powder diffraction on a Philips PW3710 diffractometer.

The impedance measurements conditions were previously described in [1]. The frequency/temperature ranges are 5–13,000 Hz/526–668 K, respectively. Pellets of 13 mm diameter and 1.82 mm thickness were prepared by pressing the powder sample at 15 tonnes and then the pellets were sintered at 773 K for 24 h. Magnetic susceptibility measurements were performed on polycrystalline samples on a Quantum Design SQUID magnetometer in the temperature range 2–300 K at 2 K intervals. Magnetic susceptibility as a function of temperature was measured in the zero-field-cooling (ZFC) and field cooling (FC) process with a magnetic field of 200 G. The data were corrected for the sample holder and for the diamagnetic contribution calculated from Pascal constants [10]. Magnetization vs. magnetic field strength M was measured at 5, 10, 20 and 40 K in a field range from −2 to 5 T.

3. Results and discussion

3.1. The crystal structure determination

The crystal data were collected on an Enarf–Nonius CAD-4 automatic four-circle diffractometer using the Mo$K\alpha$ radiation ($\lambda = 0.71069$ Å) first in the monoclinic system and this on the assumption that the compound under investigation is isostructural with $KFeP_2O_7$ [4]. The ordinary corrections; for Lorentz and polarization effects, absorption via a psi-scan [11] and secondary extinction correction [12] were applied. The crystal structure was refined in the space group $P2_1/c$. However, the obtained results present many anomalies: the reliability factors are high, $R = 0.13$ and only isotropic refinement could be performed: several of the anisotropic thermal parameters became negative. Attempts to refine the structure in other monoclinic space groups as well as a reproduction of data measurements with another crystal sample led to the same anomalies. Consequently and in a last attempt, we carried to lower the symmetry and the data collection was reproduced in the triclinic system.

A summary of the fundamental crystal data is given in Table 1. The cell parameters were determined and optimized by least-squares refinement based upon 25 reflections at the range $10.35° \leqslant \theta \leqslant 14.95°$. The systematic absences as well as the statistical tests [13] in the reduced data indicated the inversion center and the space group P-1. The crystal structure was solved and refined against F^2, all calculations were performed using the SHELX-97 [12,14] computer programs included in the WinGX software package [15]. Molecular graphics are made with Diamond 2.1 supplied by Crystal Impact [16].

The metal and arsenic atoms were first located and then all the oxygen and two potassium atoms were found by successive Fourier difference synthesis. At this stage the atomic coordinates and isotropic temperature factors were refined to $R = 0.053$ and $R_W = 0.129$. When all the atoms were anisotropically refined, the agreement factors R and R_W converged to 0.035 and 0.095, respectively; a refinement of site occupations did not show significant deviations. This time, all ADPs are positive with normal

Table 1
Summary of crystallographic data, recording conditions and structure refinement results for $KFeAs_2O_7$

Crystal data	
Empirical formula	$KFeAs_2O_7$
Crystal system; space group	Triclinic; P-1
Unit cell dimensions	$a = 7.662$ (1) Å, $b = 8.402(3)$ Å, $c = 10.100(3)$ Å $\alpha = 90.42(3)°$, $\beta = 89.74(2)°$, $\gamma = 106.39(2)°$
Volume; Z	623.8(3) $Å^3$; 4
Crystal shape; color	Parallelepiped; beige
Crystal size	$0.216 \times 0.114 \times 0.072$ mm^3
Formula weight; $\rho_{calc.}$	356.79 g mol^{-1}; 3.799 g cm^{-3}
Absorption coefficient (μ)	13.60 mm^{-1}
Data collection	
Diffractometer	Enraf-Nonius CAD-4
Wavelength; temperature	$\lambda_{Mo\ K\alpha} = 0.71069$ Å; 298(2) K
Theta range for data collection	$2.02 \leqslant \theta \leqslant 26.95°$
Limiting indices	$-2 \leqslant h \leqslant 9$; $-10 \leqslant k \leqslant 10$; $-12 \leqslant l \leqslant 12$
Scan mode	$\omega/2\theta$
Absorption correction; T_{min}; T_{max}	psi-scan; 0.170; 0.376
Standards; frequency (min); decay (%)	2; 120; 1
Reflections collected	3730
Independent reflections	2713 [$R_{int.} = 0.0210$]
Observed reflections [$I > 2\sigma(I)$]	2512
Refinement	
Refinement method	Full-matrix least-squares on F^2
Final R indices [$I > 2\sigma(I)$]	$R = 0.0351$; w$R = 0.0951$
Reflections; parameters	2713; 200
$\Delta\rho_{max}$; $\Delta\rho_{min}$ (e $Å^{-3}$)	1.466; −1.321
Extinction coefficient	0.0059(6)
Goodness of fit (S)	1.01

standard deviations and the residual peaks are near the arsenic atoms. Further details of the crystal structure investigation can be obtained from the Fachinformationszentrum Karlsruhe, 76344 Eggenstein-Leopoldshafen, Germany, (fax: (49) 7247-808-666; e-mail: crysdata@fiz.karlsruhe.de) on quoting the depository number CSD-418415.

The two structural validation tools, although with different formulations, Bond valence sums (BVS) [17–19] and charge distribution (CD) analysis [20,21] were chosen to validate the structural model. The CD analysis is mainly chosen because of the insights into the structural details (average weighted distances, effective coordination numbers (EcoNs)) that it gives at the same time. The BVS and CD show that the structure is well refined and yield adequate valences (V)/formal charges (Q) for all atoms with minor deviations from expected values.

The final atomic coordinates and thermal parameters are given in Table 2. The bond valence computation (V) and CD analysis (Q) are gathered in Table 3. The principal interatomic distances are listed in Table 4.

Table 2
Atomic coordinates and equivalent isotropic thermal factors in $KFeAs_2O_7$

Atom	Position	x	y	z	U_{eq} (Å^2)
As1	2*i*	0.15305 (8)	0.85088 (7)	0.42253 (6)	0.0062 (2)
As2	2*i*	0.43870 (7)	0.67735 (7)	0.35619 (6)	0.0059 (2)
As3	2*i*	0.12646 (8)	0.33418 (7)	0.10220 (6)	0.0059 (2)
As4	2*i*	0.45024 (8)	0.20319 (7)	0.13316 (6)	0.0065(2)
Fe1	2*i*	0.2334 (1)	0.7704 (1)	0.09972 (8)	0.0091 (2)
Fe2	2*i*	0.2345 (1)	0.2652 (1)	0.40618 (9)	0.0103 (2)
K1	2*i*	0.1604 (2)	0.5384 (2)	0.6776 (2)	0.0181 (3)
K2	2*i*	0.8179 (2)	0.9411 (2)	0.1775 (2)	0.0181 (3)
O1	2*i*	0.1035 (6)	0.8102 (6)	0.2638 (4)	0.0133 (9)
O2	2*i*	0.1861 (6)	1.0441 (5)	0.4751 (5)	0.0146 (9)
O3	2*i*	0.3615 (6)	0.8132 (5)	0.4581 (4)	0.0116 (9)
O4	2*i*	−0.0022 (6)	0.7122 (5)	0.5110 (4)	0.0100 (8)
O5	2*i*	0.6409 (6)	0.6742 (5)	0.4130 (4)	0.0117 (8)
O6	2*i*	0.2766 (6)	0.5000 (5)	0.3735 (5)	0.0153 (9)
O7	2*i*	0.4521 (6)	0.7556 (5)	0.2022 (4)	0.0115 (9)
O8	2*i*	−0.0040 (6)	0.2176 (5)	−0.0149 (4)	0.0103 (8)
O9	2*i*	0.1107 (6)	0.5256 (5)	0.1193 (4)	0.0109 (8)
O10	2*i*	0.0829 (6)	0.2220 (5)	0.2414 (4)	0.0098 (8)
O11	2*i*	0.3499 (6)	0.3425 (5)	0.0549 (4)	0.0112 (8)
O12	2*i*	0.3317 (6)	0.0178 (5)	0.0788 (5)	0.0144 (9)
O13	2*i*	0.4484 (6)	0.2432 (6)	0.2959 (4)	0.0147 (9)
O14	2*i*	0.6653 (6)	0.2592 (5)	0.0802 (4)	0.0101 (8)

U_{eq} is defined as one third of the trace of the orthogonalized U_{ij} tensor.

3.2. Structure description and discussion

The triclinic framework of the title compound is adopted by the isotypic compounds $A\mathrm{InAs_2O_7}$ (A = Tl, Rb, NH_4) [2]. There are 22 atoms in the unit cell, all in general positions. The four distinct arsenic atoms form two independent As_2O_7 groups and the two non-equivalent

Table 4
Main interatomic distances and arithmetic/weighted average distances (Å) [19,20,23] in the coordination polyedra for $KFeAs_2O_7$

As1 tetrahedron		As3 tetrahedron	
As1–O2	1.655 (4)	As3–O9	1.654 (4)
As1–O1	1.660 (4)	As3–O8	1.673 (4)
As1–O4	1.671 (4)	As3–O10	1.678 (4)
As1–O3	1.752 (4)	As3–O11	1.758 (4)
⟨As1–O⟩	1.685/1.679	⟨As3–O⟩	1.691/1.685
As2 tetrahedron		As4 tetrahedron	
As2–O6	1.658 (4)	As4–O12	1.657 (4)
As2–O5	1.662 (4)	As4–O14	1.667 (4)
As2–O7	1.684 (4)	As4–O13	1.677 (5)
As2–O3	1.753 (4)	As4–O11	1.764 (4)
⟨As2–O⟩	1.689/1.684	⟨As4–O⟩	1.691/1.685
Fe1 octahedron		Fe2 octahedron	
Fe1–O8^{vi}	1.987 (4)	Fe2–O2^{ix}	1.923 (5)
Fe1–O1	2.003 (4)	Fe2–O6	1.938 (4)
Fe1–O7	2.008 (4)	Fe2–O10	2.005 (4)
Fe1–O12^{ii}	2.014 (4)	Fe2–O4^{i}	2.019 (4)
Fe1–O14^{iv}	2.014 (4)	Fe2–O13	2.028 (5)
Fe1–O9	2.016 (4)	Fe2–O5^{vi}	2.058 (5)
⟨Fe1–O⟩	2.007/2.007	⟨Fe2–O⟩	1.995/1.987
K1 polyhedron		K2 polyhedron	
K1–O4	2.757 (5)	K2–O10^{x}	2.719 (4)
K1–O5^{v}	2.800 (4)	K2–O8^{iv}	2.744 (5)
K1–O4^{i}	2.838 (5)	K2–O7	2.808 (4)
K1–O9^{i}	2.856 (5)	K2–O1^{xi}	2.854 (5)
K1–O13^{v}	3.052 (5)	K2–O12^{iv}	2.898 (5)
K1–O14^{v}	3.057 (5)	K2–O8^{x}	3.048 (5)
K1–O1^{i}	3.113 (5)	K2–O5	3.295 (5)
K1–O10^{i}	3.206 (5)	K2–O11^{iv}	3.326 (5)
K1–O6	3.233 (5)	K2–O14^{vii}	3.360 (5)
K1–O3	3.265 (5)	K2–O2^{v}	3.510 (4)
K1–O6^{i}	3.315 (5)	⟨K2–O⟩	3.086/2.879
⟨K1–O⟩	3.045/2.958		

Symmetry transformations to generate equivalent atoms: (i) $-x$, $1-y$, $1-z$; (ii) $x-1$, y, z; (iii) $x-1$, $y-1$, z; (iv) $1-x$, $1-y$, $-z$; (v) $1-x$, $1-y$, $1-z$; (vi) $-x$, $1-y$, $-z$; (vii) x, $1+y$, z; (viii) $1-x$, $2-y$, $-z$; (ix) x, $y-1$, z; (x) $1+x$, $1+y$, z; (xi) $1+x$, y, z.

Table 3
Bond valence computation (V) and Charge distribution analysis (Q) for $KFeAs_2O_7$

	As1	As2	As3	As4	Fe1	Fe2	K1	K2	O1	O2	O3
V	5.04	4.97	4.98	4.95	3.01	3.11	1.01	0.99	−2.04	−2.02	−2.16
Q	4.92	5.05	4.93	5.16	2.97	3.00	1.00	0.98	−2.08	−2.01	−1.97
	O_4	O_5	O_6	O_7	O_8	O_9	O_{10}	O_{11}	O_{12}	O_{13}	O_{14}
V	−2.05	−1.94	−2.06	−1.91	−2.04	−1.99	−2.03	−2.11	−1.97	−1.85	−1.91
Q	−2.05	−1.96	−2.07	−1.93	−2.13	−2.03	−2.03	−1.92	−2.03	−1.85	−1.96

iron atoms are octahedrally coordinated by oxygen atoms. The overall degree of distortion of the different coordination polyhedra with respect to their regular counterparts is evaluated by both the effective coordination numbers ECoN [21–24] as well as the distortion indices ID [25] (Table 5).

The Fe1 octahedron is almost regular and the Fe2 one is slightly distorted with ECoN(Fe1) = 5.995 and ECoN(Fe2) = 5.867. The four As tetrahedra are slightly distorted as shown by the IDs and the ECoNs. A slightly O–O edge distortion ID_o is observed for $As1O_4$ as compared to the other tetrahedra (Table 5). The As1–O3–As2 and As4–O11–As3 bond angles involving the bridging oxygen atoms (116.99(2) and 119.20(2)°, respectively) are reasonably close to those in the isotypic $A InAs_2O_7$ (A = Tl, Rb, NH_4) compounds [2]. The two independent $K1$ and $K2$ positions are 4.56 Å apart along the [0 1 0] direction. They are coordinated by 11 and 10 oxygen atoms, respectively, with ECoN($K1$) = 9.349 and ECoN($K2$) = 7.310.

The two iron octahedra are not directly connected but share their corners with six tetrahedra of five different diarsenate groups. From this interconnection two non-equivalent $FeAs_2O_{11}$ units result, as observed in related structures; these are furthermore connected by common oxygen, leading to the $Fe_2As_4O_{21}$ unit. The three-dimensional anionic framework $[FeAs_2O_7^-]$ can also be described as formed by infinite anionic layers parallel to (1 0 1) plane connected via Fe–O–As bridges. This building block originates wider tunnels parallel to the b-direction hosting potassium cations (Fig. 1) and smaller tunnels parallels to [1 0 1] directions (Fig. 2). It has to be remarked an open-pore framework structure in the titled compound, that was already signaled for the isotypic compounds $A InAs_2O_7$ (A = Tl, Rb, NH_4). To this the name of MCV-4 (from the Institute of Mineralogy and Crystallography Vienna) was assigned [2].

In the following sections we discuss some relevant electrical and physical properties of the titled compound, and how these can be related to the above determined crystal structure.

Table 5
Distortion parameters ECoN and ID for the coordination polyhedra around Fe and As

	Fe1	Fe2	As1	As2	As3	As4
ECoN	5.995	5.867	3.928	3.933	3.926	3.916
ID_d	0.004	0.022	0.020	0.019	0.020	0.022
ID_a	0.031	0.054	0.039	0.037	0.035	0.040
ID_o	0.026	0.042	0.021	0.012	0.016	0.016

$ID_d = \left(\sum_{i=1}^{n1}(|d_i - d_m|)/n_1 d_m\right)$; $ID_a = \left(\sum_{i=1}^{n2}(|a_i - a_m|)/n_2 a_m\right)$; and $ID_o = \left(\sum_{i=1}^{n2}(|o_i - o_m|)/n_2 o_m\right)$ d, a, o signify Fe/As–O bond distance. O–Fe/As–O angle and O–O edge within the relevant polyhedron; index i indicates individual values, index m the mean value for the polyhedron. $n1$ and $n2$ are 4 and 6 for the phosphate tetrahedra and 6 and 12 for the iron octahedral [25].

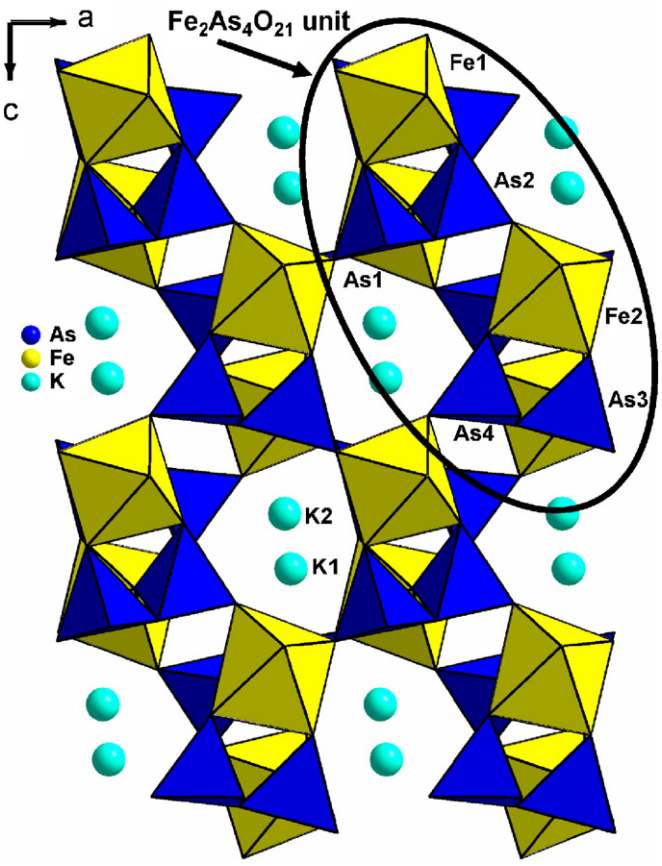

Fig. 1. Projection of the structure down the crystallographic b-axis.

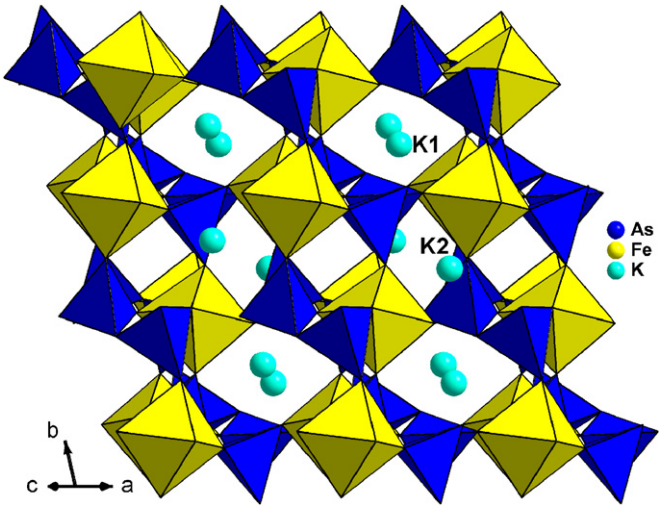

Fig. 2. Polyhedral representation of the structure showing smaller tunnels parallel to [1 0 1].

3.3. Cation transport properties

The electrical properties of the title compound have been investigated using complex impedance spectroscopy (CIS), which is an important tool to examine the electrical properties of a polycrystalline material by means of the

correlation between the sample electrical behavior and its microstructure.

The electrical conductivity generally consists of both ionic and electronic conduction. The ionic part is proportional to the ion concentration and mobility while the electronic conduction follows the hopping theory [26,27]. The electronic conductivity in oxides is due to overlapping of non-completely filled d or f orbitals of cations or to electron hopping from aliovalent ions, like Fe^{2+} and Fe^{3+} assisted by an oxygen anion in between. In the title compound the conductivity should be totally ionic, as iron shows only one valence state (FeIII). Some electronic conductivity could be present in grain boundaries, but is considered to be negligible.

The impedance plots imaginary vs. real part ($Z^* = Z' - jZ''$) recorded at various temperatures and linear plots of $\log(\sigma T)$ vs. $10^3/\mathrm{T}(\mathrm{K}^{-1})$ are shown in Fig. 3. An Arrhenius-type behavior $\sigma T = A_0 \exp(-E_a/kT)$ is shown, where A_0 and E_a are the pre-exponential factor and the activation energy, respectively. The measured impedance can be modeled by an equivalent circuit as shown in the inset of Fig. 3.

The presence of single semicircular arcs indicates that the electrical processes in the material arise basically due to the contribution from the bulk material [28,29]; it can then be modeled as an equivalent electrical circuit comprising a parallel combination of a bulk resistance (R_b) and a bulk capacitance (C_b).

The conductivity value σ at 568 K is $2.76 \times 10^{-7}\,\mathrm{S\,cm^{-1}}$ and the activation energy for K^+ ions migration deduced from the slope is $E_a = 0.47$ eV; $KFeAs_2O_7$ shows a modest ionic conductivity, comparable to those found for other diarsenates [1,30].

3.4. Conduction pathways proposed from bond valence analysis

The concept of bond valence [17–19] can be successfully used to simulate cations motion in the crystal bulk, such as lithium ion conduction in $La_{2/3-x}Li_{3x}TiO_3$ [31], sodium in Nasicon conductors [32] and in $Na_2M_2(BO_3)_2O$ (M = Al,Ga) and $Na_{2-2x}Ca_xGa_2(BO_3)_2O$ (x = 0.25,0.50) [33] and thallium in $TlFe_{0.22}Al_{0.78}As_2O_7$ [1]. In this case, the BVS model offers a useful tool to relate the novel crystal structure to its ionic conductivity properties.

Ionic pathways are calculated from BVS $\varphi(x,y,z)$ in a large grid of points starting from $K1$ and $K2$ crystallographic positions (2i), as determined by X-ray diffraction. Analysis of the lowest $\varphi(x,y,z)$ shows that low-activation energy motion occurs along certain migration directions such as tunnels connecting crystallographic sites. It has been shown that such a procedure simulates the effect of external electrical force acting on the ion [34]. Points in the ionic pathways with the lowest φ values correspond to stable positions; the highest values are associated with bottlenecks. The structural parameters resulting from X-ray analysis are assumed constant when the cations diffuse.

As in $TlFe_{0.22}Al_{0.78}As_2O_7$ [1], the K^+ motions appear to be easier only for migration direction, parallel to b-axis (Fig. 4) connecting $K1$ to $K2$ and to $K1$ again with a $K1$–$K2$ hopping distance of 4.56(4) Å. Along this direction, the maximum $\varphi(x,y,z)$ value (called hereinafter Vumax) is $\varphi(d) = 1.53$ whilst the minimum is $\varphi(d) = 0.89$. Along a and c cell directions, the ion motion seems difficult and the cations reach quickly bottlenecks: Vumax attains 1.97 and 1.94 for covered distances not exceeding 1.14 and 2.74 Å for $K1$ along [1 0 0] and [0 0 1], respectively.

The only conduction pathway is hence along tunnels parallel to b-direction, the modest ionic conductivity of this

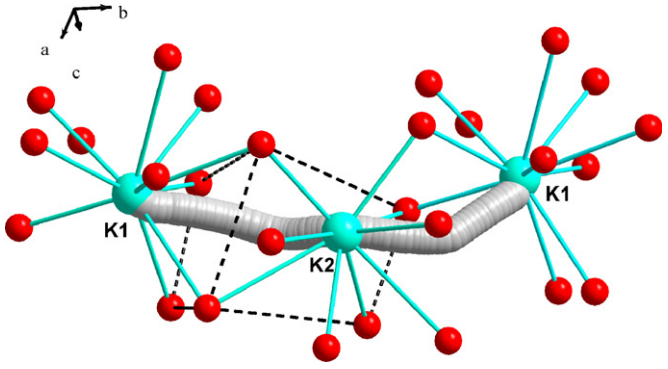

Fig. 4. Optimized trajectory for K1–K2–K1 jump.

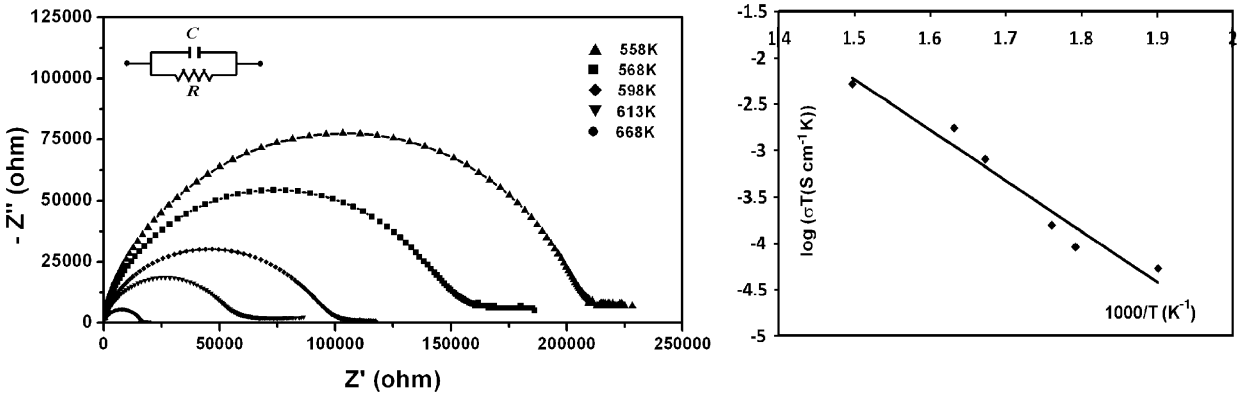

Fig. 3. Complex impedance diagrams $-Z''$ vs. Z' for $KFeAs_2O_7$ over the temperature ranges 558–668 K and Conductivity plot $\log(\sigma T) = f(10^3/T)$.

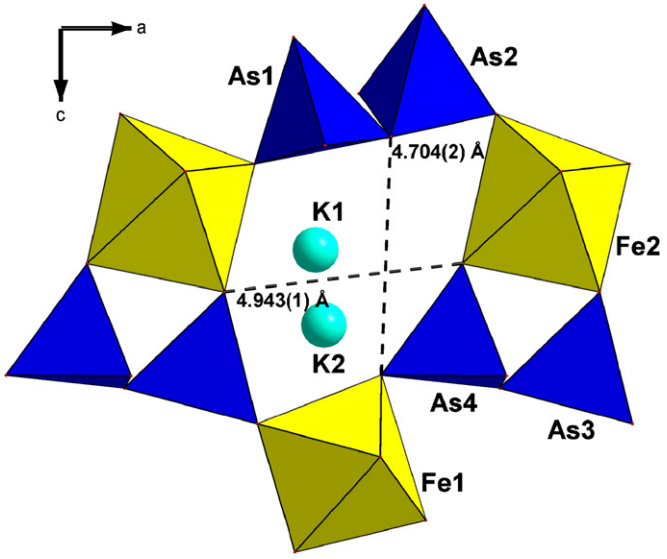

Fig. 5. View of the shape and size of the [0 1 0] tunnel sections in $KFeAs_2O_7$.

material is allotted to dimensions of the tunnels sections. The bottleneck widths of the tunnels vary from 4.704 to 4.943 Å (Fig. 5) and thus they result smaller than the geometrical size sum of 5.46 Å corresponding to $2\times(r_{K+}+r_{O2-})=2\times(1.38+1.35)$ [35]. Second, smaller tunnels, with bottleneck widths varying from 3.179 to 4.939 Å [35] and extending along [1 0 1], are not favorable for the cations mobility: bottlenecks of Vumax = 1.88 are met by the cations for a covered distance of 3.04 Å (Fig. 6).

On the basis of BVS we can conclude that the transport properties in this material appear to be due to K^+ ions movement along *K*1–*K*2 connectivity in *b*-direction.

3.5. Magnetic susceptibility

We reported in Figs. 7–9, the plots of χ_M (the molar magnetic susceptibility), $1/\chi_M$ (the inverse molar magnetic susceptibility) and $\chi_M T$ vs. the temperature T measured under the ZFC and FC process with a magnetic field of 200 G. One can deduce that $KFeAs_2O_7$ obeys the Curie—Weiss type paramagnetic behavior over the range 40–300 K. The paramagnetic data were fitted to the Curie–Weiss equation, $\chi_M=\chi_{dia}+C/(T-\theta)$, where χ_{dia} is diamagnetic susceptibility; C is the Curie constant and θ is the Weiss temperature. A least squares yielded best-fit values of $\chi_{dia}=-257\times10^{-6}$ emu mol^{-1}, $C=7.69$ emu Kmol^{-1} and $\theta=41.5$ K. From the relation $C=N\mu_{eff}^2/3k_B$ one obtains the effective magnetic moment $\mu_{eff}=5.55\,\mu_B$ per Fe^{3+}. It is slightly lower than the ideal value of $5.92\,\mu_B$ for a d^5, with theoretically expected for spin-only iron (III) ions.

To examine the ferromagnetic contributions we carried out magnetization measurements. Below T_N (29.3 K, ferromagnetic transition temperature), the variation of the magnetization with the magnetic field at 5 and 10 K shows a small hysteresis loop in which the values of the coercive field and remanent magnetization are, approximately, (250 G and 34.9 emu mol^{-1} (or $7.0\times10^{-3}\,\mu_B$ mol^{-1})) and (170 G and 24.0 emu mol^{-1} (or $4.3\times10^{-3}\,\mu_B$ mol^{-1})), respectively, and disappear at 40 K (Fig. 10).

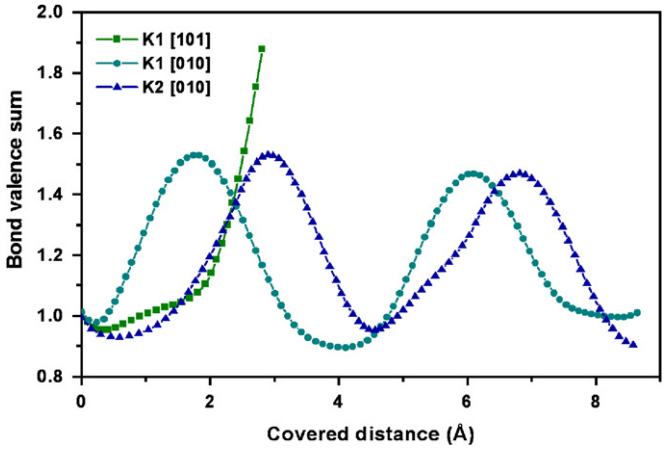

Fig. 6. Bond valence sum for potassium ions vs. the covered distance.

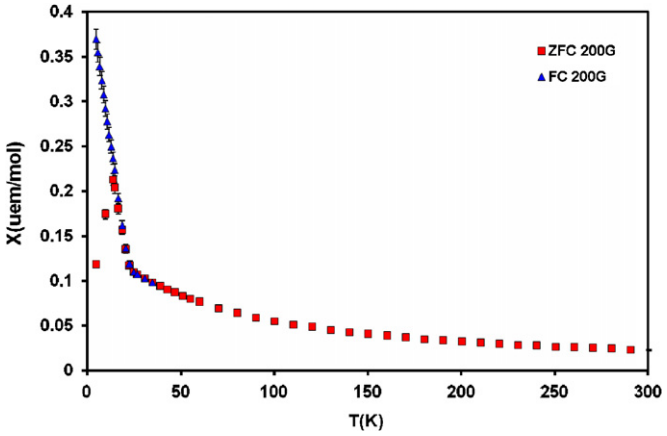

Fig. 7. Thermal variation of the molar susceptibility square for ZFC and triangle for FC for $KFeAs_2O_7$.

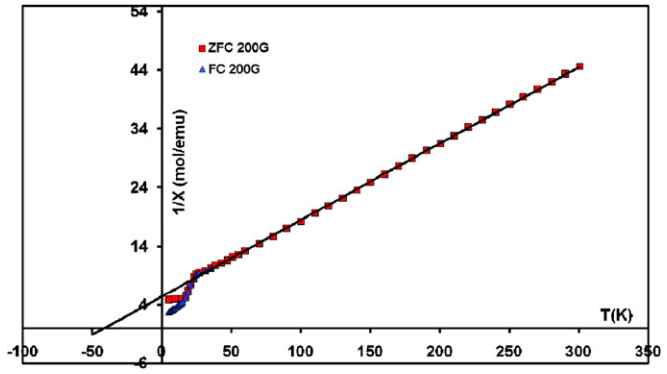

Fig. 8. Thermal variation of the inverse molar susceptibility square for ZFC and triangle for FC for $KFeAs_2O_7$.

This behavior was already observed in the substitutional solid solution $Li_3Fe_2(PO_4)_{3-x}(AsO_4)_x$ ($x = 1, 1.5, 2, 3$) [36]. It was explained by the connectivity of As, P tetrahedra involving Fe–O–(As,P)–O–Fe superexchange pathways. It was deduced that two ferromagnetic sublattices are antiferromagnetically coupled, due to the strengthening of the antiferromagnetic interaction between Fe_1 and Fe_2 ferromagnetic sublattices in that compound. For that and similar structures the crystallographically non-equivalent iron sites display different temperature dependences for the molecular field, giving rise to a phenomenon of *L*-type ferrimagnetism [37–41]. In the title compound we have a similar situation with two independent FeO_6 octahedra, symmetry unrelated, which explain the presence of a weak ferrimagnetism. However, taking into account of the magnitude of the remaining magnetization value, the misalignment of the magnetic moments may correspond only to a few of degree.

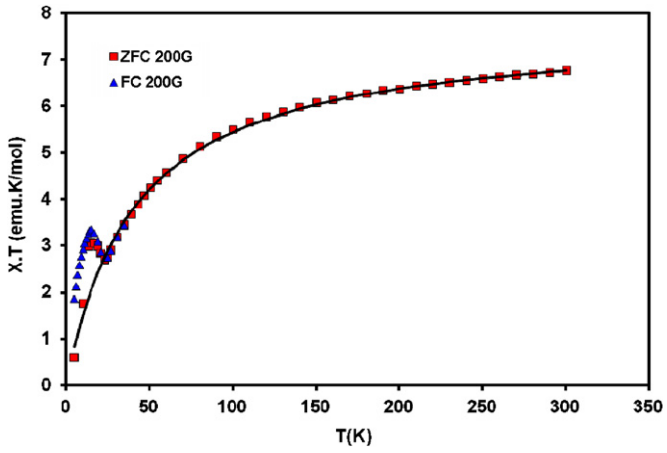

Fig. 9. Thermal variation of the molar χT product square for ZFC and triangle for FC for $KFeAs_2O_7$.

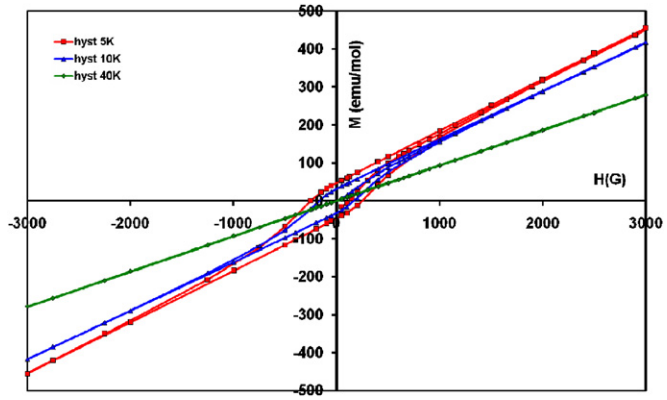

Fig. 10. Variation of the molar magnetization vs. the magnetic field measured at 5, 10 and 40 K for $KFeAs_2O_7$.

These results confirm the existence of a ferromagnetic contribution intrinsic to the sample due to strong dipolar interactions and consequently the presence of a hysteresis below T_N suggests the occurrence of a spin canting at these temperatures. This compound can be therefore classified as a weak ferrimagnetic.

3.6. Infrared spectroscopy

The infrared spectrum was recorded in the range 1200–400 cm^{-1} (Fig. 11); it reflects the complexity of the structure. The considerably large number of bands is due to the existence of four crystallographically different AsO_4 tetrahedra (two As_2O_7 groups). According to the literature [1,30,42,43], the assignment of the As_2O_7 bands is carried out in terms of AsO_3 and As–O–As group vibrations. The ν_{as}(As–O) asymmetrical stretching mode of the [AsO_4] appears at 970 and 882 cm^{-1}. The ν_s(As–O) asymmetrical stretching is detected at 845 cm^{-1}. The asymmetrical deformation vibrations [δ_{as}(O–As–O)] are observed at 484 and 468 cm^{-1}. The peaks at 601 and 764–786 cm^{-1} are attributed to symmetric (ν_s) and asymmetric (ν_{as}) As–O–As vibrations modes of the As_2O_7 group, respectively.

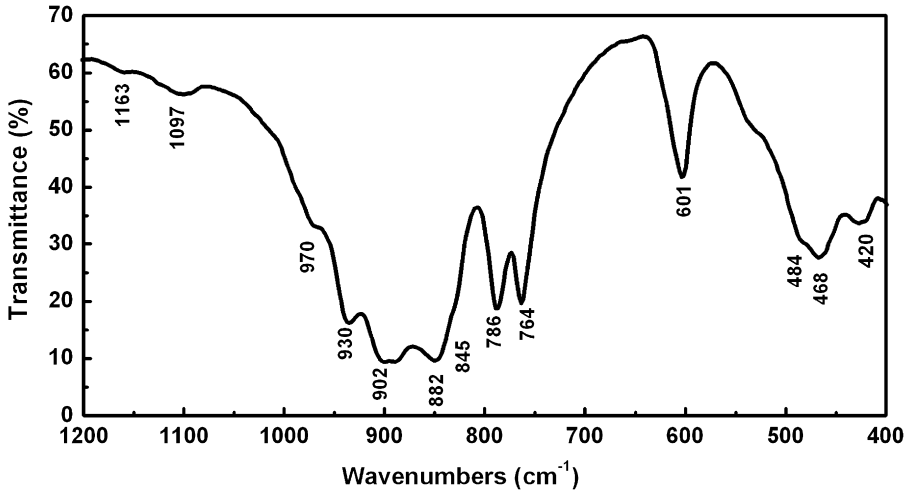

Fig. 11. Infrared analysis spectrum of $KFeAs_2O_7$.

Acknowledgment

We are grateful to the Laboratoire de Physique des Matériaux, Faculté des Sciences de Bizerte, Tunisia, for the electric measurements.

References

[1] N. Ouerfelli, A. Guesmi, D. Mazza, A. Madani, M.F. Zid, A. Driss, J. Solid State Chem. 180 (2007) 1224–1229.
[2] K. Schwendtner, J. Alloys Compds. 421 (2006) 57–63.
[3] M. Gabelica-Rpbert, M. Goreaud, Ph. Labbe, B. Raveau, J. Solid State Chem. 45 (1982) 389–395.
[4] D. Riou, Ph. Labbe, M. Goreaud, Eur. J. Solid State Inorg. Chem. 25 (1988) 215–229.
[5] U. Kolitsch, Z. Kristallogr. NCS 219 (2004) 207–208.
[6] K. Schwendtner, U. Kolitsch, Acta Crystallogr. C 60 (2004) i79–i83.
[7] N.H. Ng, C. Calvo, Can. J. Chem. 5l (1973) 2620–2673.
[8] K. Horchani-Naifer, M. Férid, Solid State Ionics 176 (2005) 1949–1995.
[9] A. Hamady, M.F. Zid, T. Jouni, J. Solid State Chem. 113 (1994) 120–124.
[10] A. Earshaw, Introduction to Magnetochemistry, Academic Press, London, 1968.
[11] A.C.T. North, D.C. Phillips, F.S. Mathews, Acta Crystallogr. A 24 (1968) 351–359.
[12] G.M. Sheldrick, SHELXS-97 a Program for Crystal Structure Determination, University of Göttingen, Germany, 1997.
[13] R.E. Marsh, Acta Crystallogr. B 51 (1995) 897–907.
[14] G.M. Sheldrick, SHELXL-97 a Program for the Refinement of Crystal Structures, University of Göttingen, Germany, 1997.
[15] L.J. Farrugia, J. Appl. Crystallogr. 32 (1999) 837–838.
[16] K. Brandenburg, M. Berndt, Diamond Version 2.1,, Crystal Impact, Bonn, 2001.
[17] I.D. Brown, Phys. Chem. Miner. 15 (1987) 30–34.
[18] Softbv web page by Pr. Stefan Adams: 〈http://kristall.uni.mki.gwdg.de/softbv〉.
[19] S. Adams, J. Maier, Solid State Ionics 105 (1998) 67–74.
[20] M. Nespolo, G. Ferraris, H. Ohashi, Acta Crystallogr. B 55 (1999) 902–916.
[21] M. Nespolo, G. Ferraris, G. Ivaldi, R. Hoppe, Acta Crystallogr. B 57 (2001) 652–664.
[22] M. Nespolo, G. Ferraris, R. Hoppe, J. Ceram. Process. Res. 2 (2001) 38–44.
[23] R. Hoppe, S. Voigt, H. Glaum, J. Kissel, H.P. Muller, K. Bernet, J. Less-Common Met. 156 (1989) 105–122.
[24] M. Nespolo, CHARDT-IT A Program to Compute Charge Distributions and Bond Valences in Non-molecular Crystalline Structures, LCM3B, University Henri Poincaré Nancy I, France, 2001.
[25] M. Wildner, Z. Kristallogr. 202 (1992) 51–70.
[26] N.F. Mott, J. Non-Cryst. Solids 106 (1968) 1–17.
[27] I.G. Austin, N.F. Mott, Adv. Phys. 18 (1969) 41–102.
[28] J.T.C. Irvine, D.C. Sinclair, A.R. West, Adv. Mater. 2 (1990) 132–138.
[29] S. Selvasekarapandian, M. Vijaykumar, Mater. Chem. Phys. 80 (2003) 29–33.
[30] N. Ouerfelli, M.F. Zid, T. Jouini, A.M. Touati, J. Soc. Chim. Tunisie 6 (2004) 85–97.
[31] D. Mazza, S. Ronchetti, O. Bohnké, H. Duroy, J.L. Fourquet, Solid State Ionics 149 (1–2) (2002) 81–88.
[32] D. Mazza, J. Solid State Chem. 156 (2001) 154–160.
[33] G. Corcel, D. Mazza, O. Bohnké, M. Leblanc, Solid State Sci. 7 (2005) 588–593.
[34] D. Mazza, J. Solid State Chem. 156 (1) (2001) 154–160.
[35] R.D. Shannon, Acta Crystallogr. A 32 (1976) 751–764.
[36] A. Goñi, J.L. Mesa, J.L. Pizarro, L. Fournés, A. Wattiaux, R. Olazcuaga, M.I. Arriortua, T. Rojo, J. Solid State Chem. 179 (2006) 81–90.
[37] G.L. Long, G. Longworth, P. Battle, A.K. Cheetham, R.V. Thundathil, D. Beveridge, Inorg. Chem. 18 (1979) 624–632.
[38] P.D. Battle, A.K. Cheeetham, G.J. Long, G. Longworth, Inorg. Chem. 21 (1982) 4223–4228.
[39] P.D. Battle, A.K. Cheethem, W.T.A. Harrison, G.J. Long, J. Solid State Chem. 62 (1986) 16–25.
[40] L. Néel, Ann. Phys. (Paris) 3 (1948) 137.
[41] T. Moya-Pizarro, R. Salmon, L. Fournes, G. LeFlem, B. Wanklyn, P. Hagenmuller, J. Solid State Chem. 53 (1984) 387–397.
[42] N. Stock, G.D. Stucky, A.K. Cheetham, J. Phys. Chem. Solids 62 (2001) 1457–1467.
[43] R. Hubin, Spectrochem. Acta 24A (1971) 311–319.